In-situ X-ray photoelectron spectroscopy studies of water on metals and oxides at ambient conditions

S Yamamoto[1], H Bluhm[2], K Andersson[1,3,6], G Ketteler[4,7], H Ogasawara[1], M Salmeron[4,5] and A Nilsson[1,3]

[1] Stanford Synchrotron Radiation Laboratory, P.O.B. 20450, Stanford, CA 94309, USA.

[2] Lawrence Berkeley National Laboratory, Chemical Sciences Division, Berkeley, CA 94720, USA.

[3] FYSIKUM, Stockholm University, AlbaNova University Center, SE-106 91 Stockholm, Sweden.

[4] Lawrence Berkeley National Laboratory, Materials Sciences Division, Berkeley, CA 94720, USA.

[5] Department of Materials Science and Engineering, University of California, Berkeley, CA 94720, USA.

E-mail: nilsson@slac.stanford.edu

Running head: In-Situ XPS studies of water on metals and oxides at ambient conditions

[6] Present address: Center for Individual Nanoparticle Functionality (CINF), Department of Physics, Technical University of Denmark, Fysikvej 312, DK-2800 Kgs. Lyngby, Denmark.

[7] Present address: Department of Applied Physics, Chalmers University of Technology, SE-412 96 Göteborg, Sweden.

Abstract. X-ray photoelectron spectroscopy (XPS) is a powerful tool for surface and interface analysis, providing the elemental composition of surfaces and the local chemical environment of adsorbed species. Conventional XPS experiments have been limited to ultrahigh vacuum (UHV) conditions due to a short mean free path of electrons in a gas phase. The recent advances in instrumentation coupled with third-generation synchrotron radiation sources enables in-situ XPS measurements at pressures above 5 Torr. In this review, we describe the basic design of the ambient pressure XPS setup that combines differential pumping with an electrostatic focusing. We present examples of the application of in-situ XPS to studies of water adsorption on the surface of metals and oxides including Cu(110), Cu(111), TiO_2(110) under environmental conditions of water vapor pressure. On all these surfaces we observe a general trend where hydroxyl groups form first, followed by molecular water adsorption. The importance of surface OH groups and their hydrogen bonding to water molecules in water adsorption on surfaces is discussed in detail.

1. Introduction

Water adsorption on solid surfaces is ubiquitous in nature and technology, which makes the study of water at the vapor-solid or liquid-solid interfaces highly interdisciplinary. Interfacial water is a topic of research in a surprisingly wide range of scientific fields including heterogeneous catalysis [1-3], environmental science [4, 5], atmospheric chemistry [6, 7], electrochemistry [8-10], corrosion chemistry [11], and biology [12, 13]. The presence of water on surfaces has a significant influence on the mechanisms and kinetics of surface chemical processes. Adsorbed water molecules on surfaces can be a participant or spectator in surface chemical reactions. For example, water is a reactant or product in many heterogeneous catalytic reactions such as water-gas shift ($CO + H_2O \rightarrow CO_2 + H_2$) reaction or water formation reaction from oxygen and hydrogen on a platinum surface [1, 2]; traces of H_2O can promote a CO oxidation reaction on Pt(111) [14] and on Au nanoparticles supported on TiO_2 [15]. All surfaces of importance to environmental problems are covered by water with thicknesses ranging from a few Å (e.g., water vapor on aerosol particle surfaces in the upper troposphere) to infinite thickness (e.g., particles in bulk solution). Surprisingly, the growth of water on most surfaces – metallic, oxide, biological and mineral – is still poorly understood.

The interaction of water with solid surfaces has been extensively studied using surface science techniques in ultra-high vacuum (UHV) and at low temperatures, which has provided detailed information on the water/solid interface at a molecular level [16-18]. Yet most processes of interest in real systems take place at ambient or higher pressures and elevated temperatures. There is a fundamental question as to whether the information obtained at ideal conditions (UHV and low temperatures) can be extrapolated to realistic conditions (ambient pressures and high temperatures). The surface structure and surface chemical compositions in equilibrium with ambient pressure vapor can be very different from those in UHV. In addition, chemical reactions with high activation barrier can be kinetically hindered at low temperatures. These important issues are often referred to as the "pressure gap" and "temperature gap", respectively. Therefore, in order to obtain molecular-level insight into surface chemical reactions involving water, it is essential to investigate the adsorbed state and structure of water molecules on surfaces in-situ under the reaction conditions.

X-ray photoelectron spectroscopy (XPS) is a powerful experimental tool for surface science studies due to its high surface and chemical sensitivity. XPS provides information on the elemental compositions and the local chemical environment around a specific atomic site on surfaces [19-21]. The application of XPS to studies of surfaces at elevated (Torr) pressures is not straightforward due to elastic and inelastic scattering of the emitted photoelectrons by gas molecules. Conventional XPS experiments have thus been limited to UHV conditions.

In the present review, we first discuss how we overcome the obstacles in in-situ XPS by describing the synchrotron-based ambient pressure XPS system at the Molecular Environmental Science (MES) beamline at the Advanced Light Source (ALS) in Berkeley that combines differential pumping with an electrostatic focusing. We then present examples of the application of ambient pressure XPS to the study of water adsorption on metal and metal oxide surfaces under ambient conditions. The examples of in-situ XPS studies presented in this review are based on our recent experimental results on water adsorption on two different Cu surfaces of (110) and (111)

orientations [22-24] and the TiO_2(110) surface [25]. We will also give an outlook of future applications of in-situ XPS to water on surfaces.

2. Experimental

In order to perform in-situ XPS under ambient pressure vapor, one needs to reduce the attenuation of the photoelectron signal due to scattering with gas phase molecules. The attenuation of the photoelectron signal in a gas environment is proportional to exp(-zσp/kT), with σ as the electron scattering cross section, and where z represents the distance that the electrons travel through a volume at pressure p. The path length of the electrons through a gas has to be minimized. The sample surface is thus placed close to a differentially-pumped aperture, behind which the pressure drops by several orders of magnitude. This general approach has been used, beginning with Hans Siegbahn and coworkers' early designs in the 1970's [26-28], in all high-pressure XPS instruments that have been designed to date [29-37].

Ambient pressure XPS setups also have to take into account that the X-ray source (synchrotron or X-ray anode) and the electron analyzer have to be kept under high vacuum. The X-ray source is usually separated from the ambient pressure region either by differential pumping or by use of X-ray transparent windows, e.g. aluminum or silicon nitride membranes. The electron analyzer is kept under high vacuum using differential pumping between the sample cell and the analyzer. For typical aperture dimension in the range of 0.1 – 10 mm^2, typical pressure differentials across apertures vary from 10^{-4} – 10^{-2}, respectively, depending on pumping speed and the type of gas pumped. To achieve ultrahigh vacuum in the analyzer part of the chamber for pressures in the Torr range in the sample cell, several differential pumping stages are required. Depending on the aperture sizes and their relative spacing, the solid angle for collection of electrons is reduced. The smaller the apertures and the farther they are spaced apart, the more efficient is the differential pumping. However, the inverse holds for the count rate as a function of aperture size and spacing. Traditionally, the effective pressure limit in ambient pressure XPS has therefore been about 1 Torr. The recent development of ambient pressure XPS instruments that use a differentially-pumped electrostatic lens system has overcome this limitation. In these instruments, the electrons are focused onto the apertures by electrostatic lenses that are located in the differential pumping stages [35]. These systems can operate at pressures above 5 Torr (the vapor pressure of water at the triple point is 4.6 Torr) [35]. There are three instruments based on this principle currently in operation, all at third-generation synchrotron facilities (ALS beamline 9.3.2 [35]; ALS beamline 11.0.2 [36]; BESSY [37]).

The experiments described here were performed at beamline 11.0.2 at the ALS in Berkeley. This beamline uses photons from an elliptically polarizing undulator with a 5 cm period [38] and provides photons in the energy range from 75 to 2150 eV using a SX700 style plane-grating monochromator [39, 40], which is equipped with two gratings (150 and 1200 lines/mm). The Kirkpatrick-Baez (KB) mirrors (horizontal and vertical) are able to focus the spot in the experimental chambers down to below 20x20 μm^2. This is an advantage for ambient pressure XPS experiments since the entrance aperture of the differential pumping system can be kept small (i.e., provide a high pressure differential between the ambient pressure chamber and the first differentially-pumped stage) without

losing signal.

A schematic of the ambient pressure XPS spectrometer at ALS beamline 11.0.2 is shown in figure 1. The key part of the spectrometer is the differentially-pumped electrostatic lens system that separates the ambient pressure chamber from the hemispherical electron analyzer (Phoibos 150, Specs). Incident X-rays from the beamline are admitted to the ambient pressure chamber through a silicon nitride window (thickness 100 nm, active window area 1x1 mm^2). The sample is placed at a distance of ~0.5 mm from the entrance aperture (diameter 0.3 mm) to the differentially pumped lens system. Electrons and gas molecules escape through this aperture into the differentially-pumped lens system. The electrons are focused in the first differential pumping stage onto a second aperture (diameter 2 mm), and in the second differential stage onto a third aperture, also with a 2 mm diameter, before entering a final lens stage and being eventually focused onto the entrance slit of the hemispherical analyzer. The pressure differential between the ambient pressure chamber and the hemisphere is about 8 orders of magnitude.

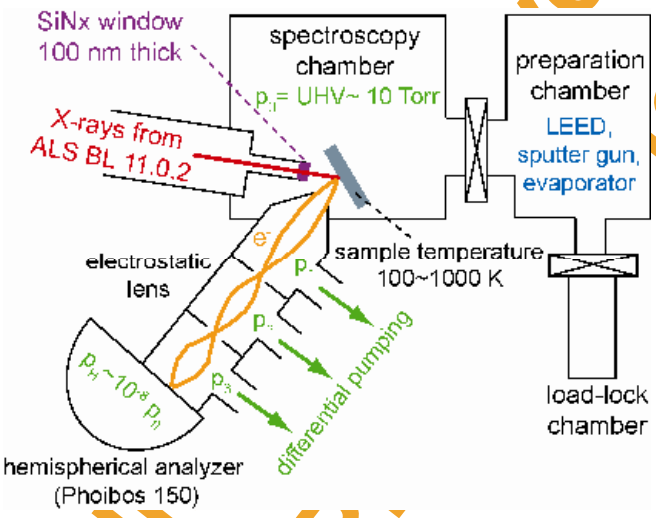

Figure 1. A schematic of the ambient pressure XPS spectrometer at ALS beamline 11.0.2

For the investigation of samples in a controlled humidity atmosphere up to the condensation point of water, the sample surface has to be the coldest point in the chamber. We have developed a transferable sample holder cooled by a two-stage Peltier element, which is isolated from the chamber atmosphere. This sample holder, combined with a stand-alone chiller for temperature control of the sample holder docking station which acts as a heat sink for the hot side of the Peltier element, allows control of the sample temperature from 220 to 350 K. For surface-science-type experiments, a button heater combined with liquid nitrogen cooling provides the temperature range from 100 to 1000 K. Besides the ambient pressure chamber, the ambient pressure XPS endstation has a preparation chamber which is equipped with a sputter gun, low-energy electron diffraction (LEED) and an evaporator for thin film deposition. A load-lock chamber allows fast exchange of samples. The base pressure in the ambient pressure and preparation chamber is $2x10^{-10}$ Torr.

Here we briefly describe the experimental procedures used in the present study of water adsorption on metals and oxides. Further experimental details are found elsewhere [22-25]. The sample surfaces of Cu(110), Cu(111), and TiO_2(110) were prepared in UHV by standard sputtering and annealing procedures as described in Ref. [22-25]. A monolayer (ML) is defined as one molecule per unit cell, i.e., $1.08x10^{15}/cm^2$ for Cu(110), $1.77x10^{15}/cm^2$ for Cu(111), and $5.2x10^{14}/cm^2$ for TiO_2(110), respectively.

Quantification of surface species under ambient pressure vapor is challenging because the intensity of a photoelectron peak is attenuated by gas-phase molecules. It should be noted that both gas-phase attenuation and transmission of electrons through the lens optics are energy-dependent. In order to obtain the coverage of O-containing species on Cu surfaces, we take the ratio of the O 1s and Cu 3p XPS peaks that are measured with identical electron kinetic energies to cancel out the gas-phase attenuation and lens transmission function. Then we calibrate it against the O 1s/Cu 3p ratio for the p(2×1)-O/Cu(110) (θ=0.5 ML) prepared in UHV [41, 42]. The coverage of O-containing species on TiO_2(110) at ambient conditions is obtained from the comparison of the absolute intensity on TiO_2(110) with that of a know coverage on Cu(110) [25].

The amount of adventitious carbon contamination on sample surfaces is negligible under UHV conditions. However, experiments under Torr pressure of water vapor cause an increased rate of contamination accumulation on surfaces. This is due to the fact that the chamber volume is virtually without pumping during ambient pressure experiments (the valve to the turbo pump needs to stay closed at ambient pressures). Sources for contaminations on the surfaces are displacement of contaminants by water at the chamber wall or the water source itself (prepared by 3 cycles of freeze-pump-thaw). We have monitored the C 1s region at all times in our experiments and have specified the amount of C contaminations simply by using the C 1s to O 1s XPS ratio measured on the C_xO_y-species with known x:y ratio. Contamination is minimized when the experiments are performed rapidly after exposure of the surfaces to water vapor, with frequent sample cleaning cycles between water exposure experiments.

3. Results

3.1 Water on metals

3.1.1 Introduction

Here we shall briefly sum up the information on the adsorbed states of water on Cu(110) and (111) surfaces obtained in previous UHV studies. On the closed-packed Cu(111) surface, water is adsorbed molecularly intact and desorbs around 160 K without dissociation [43, 44]. On the corrugated Cu(110) surface, molecular adsorption is observed at low temperatures below 150 K. Above 150 K, however, thermally-induced water dissociation is observed on Cu(110) [45]. The intact water monolayer desorbs around 170 K in kinetic competition with dissociation, forming mixed H_2O:OH phases [45]. The mixed H_2O:OH phases on Cu(110) under UHV conditions can be generated thermally, by X-ray and electron-induced damage, by coadsorption of H_2O with small amounts of atomic O, or by reacting adsorbed atomic O with atomic H, see e.g. Refs[45-53]. These mixed phases show a varying and complex temperature programmed desorption (TPD) profile depending on sample preparation and heating rate [48, 52, 53]. The main features in TPD from the mixed phases are H_2O (m/e = 18) desorption peaks at

about 200, 235 and 290 K [48, 52]. The 200 K and 235 K peaks are assigned to H_2O desorption from mixed H_2O:OH phases [48, 52]. Above 235 K, only a pure OH phase exists on the surface [48-52, 54]. This phase decomposes near 290 K via an OH recombination reaction ($OH_{ads} + OH_{ads} \rightarrow H_2O_{gas} + O_{ads}$) [48], where water desorbs with leaving behind an atomic O coverage half that of the initial OH coverage in the pure OH phase.

We will show the connection between the adsorbed states of water on two different Cu surfaces of (110) and (111) orientations under elevated water pressures and temperatures ($p(H_2O)$= 1 Torr, T= 268 – 518 K), using ambient pressure XPS, with UHV studies. One essential question is whether the results at low pressures and temperatures can be extrapolated to ambient conditions.

3.1.2 Water chemistry on Cu(110) at near ambient conditions

First we show in-situ O 1s XPS spectrum on Cu (110) measured in 1 Torr water vapor at 295 K (figure 2). In the O 1s XPS spectrum, two spectral features are observed. A strong and sharp peak at 535.75 eV binding energy (BE) is attributed to gas phase water molecules within the excitation volume in front of the entrance aperture. A broad peak with two maxima at 534 – 530 eV BE originates from H_2O and OH species adsorbed on the Cu(110) surface, as discussed below. Thus the surface signal is shifted to lower binding energies by 2 – 5 eV as compared to the gas phase signal. The large chemical shift due to the final state effects [21] allows a clear distinction between the gas phase and the surface contributions. Hereafter we only show the contributions from surface species for clarity.

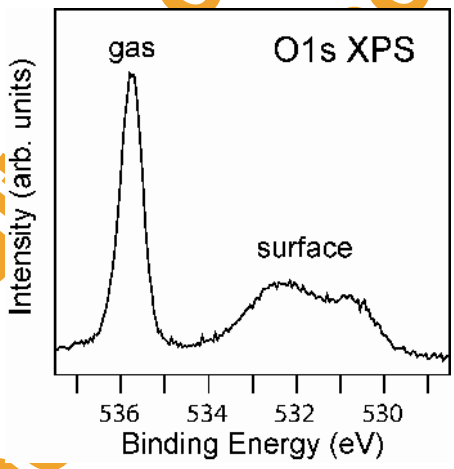

Figure 2. O 1s XPS spectrum on Cu(110) in 1 Torr water vapor at 295 K.

Next we show how the chemical composition on the Cu(110) surface changes as a function of temperature under near ambient pressure water vapor. Figure 3 shows O 1s XPS spectra measured on Cu(110) in the presence of 1 Torr water vapor at the temperature range of 275 – 518 K. The O 1s XPS features observed under 1 Torr H_2O are compared with those reported in earlier UHV studies at low temperatures. This leads to the assignment of XPS peaks observed at near ambient conditions to specific surface species.

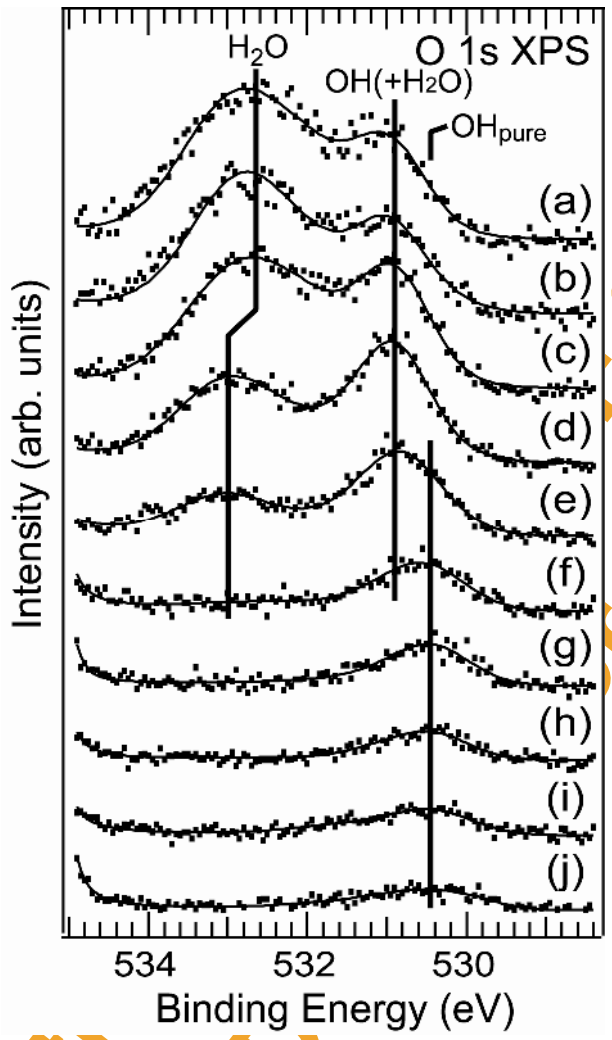

Figure 3. O 1s XPS spectra measured on Cu(110) in the presence of 1 Torr water vapor at sample temperatures of 275 – 518 K: (a) 275 K, (b) 301 K, (c) 323 K, (d) 348 K, (e) 378 K, (f) 428 K, (g) 453 K, (h) 483 K, (i) 498 K and (j) 518 K. The gas phase water peak is observed around 536 eV (not shown). The marked spectral features for "$OH(+H_2O)$" and "OH_{pure}" are for OH species H-bonding with H_2O or not, respectively. The dots are the experimental data and the thin solid line is the result from a least-square peak-fitting procedure. The incident photon energy was 735 eV.

At the lowest temperature of 275 K (figure 3a), two broad peaks are observed around 532.8 and 531.0 eV. These energies are in good agreement with previously observed O 1s XPS BEs of H_2O and OH in the mixed H_2O:OH phases on Cu(110) under UHV and low temperature conditions [45, 50, 54, 55]. Therefore the O 1s peaks around 532.8 and 531.0 eV are assigned to H_2O and OH, respectively. As the sample temperature increases, the O 1s XPS peak of adsorbed water decreases in intensity and shifts to higher BE by ~0.4 eV at temperatures between 323 K (figure 3c) and 348 K (figure 3d). Molecular water is present on the Cu(110) surface in 1 Torr H_2O up to 428 K (figure 3f). After desorption of molecular water at temperatures above 428 K (figure 3g-j), only one peak due to OH

species is observed in the O 1s XPS spectra. The binding energy of this OH species is ~0.5 eV lower than that of OH species observed when water is present on the surface at lower temperatures. The intensity of the O 1s XPS peak for OH species further decreases with an increase in temperature (figure 3f-j).

In order to obtain quantitative insights into the water chemistry on Cu(110) at near ambient conditions, the partial coverage of surface species is derived by a least-square peak fitting procedure on O 1s XPS spectra. The O 1s XPS spectra presented in figure 3 are well fitted with four components at 532.90, 532.55, 530.95, and 530.45 eV [23]. The first two components (at 532.90 and 532.55 eV BE) and the latter two (at 530.95, and 530.45 eV BE) are attributed to H_2O and OH, respectively, as discussed below; the different binding energies of the same chemical species (H_2O or OH) reflect the different molecular environments of H_2O or OH on the metal surface. To show the change in molecular environments of H_2O or OH on the Cu(110) surface, the total coverage of H_2O (i.e., 532.90 and 532.55 eV) and the coverages of two different OH components on Cu(110) under 1 Torr water vapor are plotted as a function of temperature (figure 4).

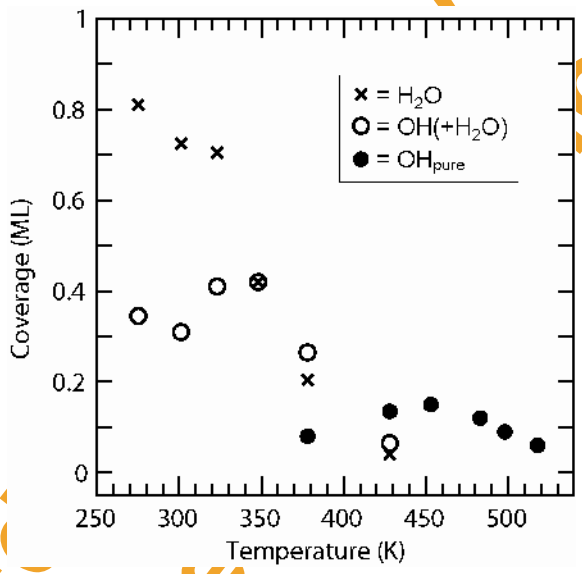

Figure 4. Partial coverages for surface species on Cu(110) in the O 1s XPS spectra presented in figure 3 recorded at 1 Torr partial pressure of H_2O and sample temperatures of 275 – 518 K. Note the identical coverage of "H_2O" (crosses) and "$OH(+H_2O)$" (open circles) at 348 K. The nomenclature used for the OH species, "$OH(+H_2O)$" and "OH_{pure}" (filled circles), are for OH species H-bonding with H_2O or not, respectively.

At lower temperatures between 275 and 323 K, the Cu(110) surface is covered to a saturation (i.e., 1 ML) with the mixed H_2O and OH layer where the ratio of H_2O to OH is 2:1[1][footnote_1]. When the sample temperature increases to 348 K, the coverage of water decreases and the H_2O:OH ratio is decreased from 2:1 to 1:1. Upon transition of the

[1] [footnote_1] At the lowest temperature of 275 K and $p(H_2O)$= 1 Torr (figure 3a), the H_2O:OH ratio is slightly larger than 2:1 (see figure 4). This may indicate the presence of small quantities of H_2O on top of the 2:1 H_2O:OH phase.

surface phase from a 2:1 to a 1:1 H_2O:OH mixed phase, the binding energy of H_2O shifts from 532.55 eV to 532.90 eV. We thus conclude that there exist two different H_2O:OH mixed phases which exhibit a large chemical shift of ~0.4 eV in the O 1s XPS peak of adsorbed water; one is with a 2:1 H_2O:OH ratio (H_2O BE: 532.55 eV) and the other is with a 1:1 H_2O:OH ratio (H_2O BE: 532.95 eV). Note that the binding energy of OH species stays close to 530.95 eV in the surface phase transition from a 2:1 to a 1:1 H_2O:OH mixed phase. With a further increase in temperature, the coverage of water continues to decrease while the H_2O:OH ratio remains close to 1:1. Molecular water is observed on the surface in the 1:1 H_2O:OH phase up to 428 K under 1 Torr H_2O, corresponding to a relative humidity (RH) as low as 2.5×10^{-2} %. The RH is defined as $p/p_v(T)\times100$, where p_v is the equilibrium vapor pressure of bulk water or ice at the corresponding temperature. When the sample temperature reaches to 378 K, a new spectral feature appears at 530.45 eV as a shoulder in the lower binding energy side of OH peak. This new peak becomes the only distinct spectral feature observed in the temperature range 453 – 518 K, where no molecular water is adsorbed on the surface. We thus assign this new feature to the OH species that are not H-bonded with water molecules. Hereafter, we refer to the OH species that are H-bonded to water (530.95 eV BE) as "OH(+H_2O)" and the OH species that are not H-bonded to water (530.45 eV BE) as "OH_{pure}". Note that both "OH(+H_2O)" and "OH_{pure}" species coexist on the surface at temperatures between 378 and 428 K. The total coverage of OH (i.e., "OH(+H_2O)" and "OH_{pure}") decreases with an increase in temperature above 378 K.

In previous UHV studies at low temperatures [45, 50, 54, 55], the binding energies of H_2O and OH were reported as follows: 530.3 – 530.6 eV for the pure OH species ("OH_{pure}"), 530.8 – 531.0 eV for the OH species that are H-bonded to water ("OH(+H_2O)"), and 532.4 – 532.9 eV for water molecules that are H-bonded to OH ("H_2O (+OH)"). These binding energies in UHV at low temperatures are in excellent agreement with those of H_2O and OH observed at near ambient conditions in the present study; 530.45 eV for "OH_{pure}", 530.95 eV for "OH(+H_2O)", 532.90 and 532.55 eV for "H_2O(+OH)".

To summarize, three different phases were observed on the Cu(110) surface under 1 Torr water vapor in the temperature range 275 – 518 K: A 2:1 H_2O:OH mixed phase, a 1:1 H_2O:OH mixed phase, and a pure OH phase, in increasing order of stability.

3.1.3 Comparison with the previous UHV studies at low temperatures

We have gained quantitative insights into the surface phases on Cu(110) under equilibrium with water vapor of near ambient pressure at elevated temperatures. We have found that there is a close correspondence in XPS binding energies of surface species between our results at near ambient conditions and the previous UHV studies at low temperatures. This indicates that the local chemical environments of H_2O and OH species are very similar at near ambient conditions and in UHV at low temperatures. Here we further discuss the similarities and differences between our results at near ambient conditions and the previous UHV studies at low temperatures, particularly regarding the surface phases, and their relative stability.

First we compare the surface phases and their relative stability at near ambient conditions with those in the previous UHV studies at low temperatures. At near ambient conditions, we observe three different phases on Cu(110) in the following order of stability; 2:1 H_2O:OH < 1:1 H_2O:OH < OH_{pure}. The previous UHV studies

reported the following surface phases in increasing order of stability; intact H_2O < 2:1 H_2O:OH <1:1 H_2O:OH < OH_{pure} < O [48, 52]. Therefore, the order of stability of three phases observed at near ambient conditions, 2:1 H_2O:OH <1:1 H_2O:OH < OH_{pure}, is fully consistent with that observed in UHV at low temperatures.

In contrast to UHV conditions, no statistically significant amount of atomic O is observed under 1 Torr H_2O in the temperature range 275 – 518 K. This can be understood by the fact that the O formation via OH_{pure} + OH_{pure} → H_2O_{gas} + O_{ads} is fast above 290 K in UHV [48-50, 55], while the reverse reaction H_2O_{gas} + O_{ads} → OH_{pure} + OH_{pure} is very facile for the O coverages below 0.15 ML even at 150 K [48-50, 55]. At near ambient conditions, therefore, the reaction equilibrium between OH and O is strongly shifted towards the OH side due to the presence of water vapor. Indeed, only atomic O is observed on the Cu(110) surface at low water partial pressures ≤ 1×10^{-4} Torr and temperatures above 300 K (not shown).

As for OH species, we find the maximum coverage of adsorbed OH to be 0.42 ML (see figure 3d and figure 4), but most frequently it saturates between 0.33 – 0.35 ML in the mixed H_2O:OH phases. These values are higher than the previously reported OH saturation coverage of 0.25 ML, which was generated by H_2O + O coadsorption on Cu(110) at low temperatures in UHV [48, 55]. Note that the high coverage of OH at near ambient conditions remains on the surface in vacuum after evacuation of water vapor if the sample temperature is below 290 K, where an OH recombination reaction becomes facile. The difference in the saturation coverage of OH may originate from the difference in the formation route of OH, i.e., thermally-induced water dissociation or preadsorbed oxygen mediated water dissociation.

So far we have established the close correlation between our results at near ambient conditions and the earlier UHV studies at low temperatures in terms of XPS binding energies of surface chemical species, the surface phases, and their order of stability. Next we will check if the surface phases observed at near ambient conditions can be explained using the kinetic information available from the previous UHV studies. Here we focus on the 1:1 H_2O:OH phase on Cu(110) observed at 428 K in 1 Torr water vapor (figure 3f), with a low water coverage of 0.04 ML.

At thermodynamic equilibrium, the rate of adsorption is equal to the rate of desorption. The rate of desorption for 0.04 ML H_2O in the 1:1 H_2O:OH phase on Cu(110) at 428 K and $p(H_2O)$= 1 Torr is evaluated based on the kinetic information available in UHV. In UHV, the H_2O desorption from the 1:1 H_2O:OH phase on Cu(110) is observed at 235 K and exhibit almost no coverage dependence, which validates the assumption of first-order desorption kinetics [48, 52, 53]. The desorption barrier for H_2O in the 1:1 H_2O:OH phase is thus calculated to be 0.69 ± 0.045 eV, using the TPD data [48] and the experimentally determined range for the pre-exponential factor (υ) for H_2O of $10^{15\pm1}$ s^{-1} [56-59]. On the basis of this desorption barrier, we obtained a H_2O desorption rate of 0.97 – 8.3×10^5 ML s^{-1} as calculated from the first-order Polanyi-Wigner equation [60]. On the other hand, the rate of adsorption is expressed as a product of an impingement rate and a sticking probability. The impingement rate under 1 Torr water vapor is calculated to be 4.3×10^5 ML s^{-1} [61]. In consequence, the desorption rate of H_2O obtained above matches well with the rate of adsorption resulting from the sticking probability close to unity. Equally good agreement is reached for the data at T = 378 K and $p(H_2O)$= 1 Torr (figure 3e).

The presence of OH groups on the surface is essential to explain the amount of adsorbed water at near ambient

conditions. Here we estimate the hypothetical desorption rates for 0.04 ML H_2O on Cu(110) observed at 428 K and $p(H_2O)$= 1 Torr if we assume that these water molecules exist in the form of monomers or clusters where water molecules are in 2-dimensional H-bonding network. The adsorption energy, i.e. the desorption barrier, of water monomers on Cu(110) has been calculated to be 0.375 eV [62]. The hypothetical desorption rate for 0.04 ML H_2O monomers on Cu(110) at 428 K is calculated using the first-order Polanyi-Wigner equation to be $1.5 \times 10^{9 \pm 1}$ ML s^{-1}. In the case of water monolayer on Cu(110), the desorption barrier is experimentally determined to be ~0.52 eV [45], corresponding to a desorption rate of $3.0 \times 10^{7 \pm 1}$ ML s^{-1}. The desorption rate of water in 2-dimensional H-bonding network is thus largely decreased as compared with that of water monomers due to an attractive H_2O-H_2O H-bonding interaction. However, the desorption rates derived from the desorption barriers for water monomer and water monolayer are significantly higher than the impingement rate under 1 Torr water vapor. In the absence of surface OH groups, therefore, we would not expect to observe any water by ambient pressure XPS (detection limit ~0.01 ML) on the Cu(110) surface. The surface OH groups act as anchoring and clustering sites for H_2O, slowing down the water desorption rate (i.e., increasing its surface residence time) drastically.

From the comparisons between our results at near ambient conditions and the previous UHV studies at low temperatures, we find a very good agreement in the local chemical environments (XPS binding energies), H_2O:OH ratios, and relative stability of the observed phases on the Cu(110) surface. The adsorption-desorption equilibrium kinetic consideration shows that the kinetic information obtained at UHV and low temperatures conditions is well extrapolated to the present conditions of elevated pressures and temperatures. Furthermore, it shows that surface OH groups play an essential role in water adsorption on the metal surface through strong hydrogen bonds that stabilize water molecules. The importance of surface OH groups in water adsorption is further demonstrated below by a clear cut example on the Cu(111) surface.

3.1.4 Water adsorption on Cu(111) at near ambient conditions

Here we show that the Cu(111) surface exhibits a very different wetting behavior than the Cu(110) surface at near ambient conditions. Figure 5 shows O 1s XPS spectra measured on Cu(110) and Cu(111) in the presence of 1 Torr water vapor at 295 K, corresponding to 5.0 % RH. The Cu(110) surface is covered with a saturated monolayer of the mixed H_2O and OH phase, as also shown in figure 2 and figure 3. In contrast, the Cu(111) surface remains clean and adsorbate-free under the identical condition. No adsorbate is observed on Cu(111) under 1 Torr H_2O vapor in the temperature range from 333 to 268 K, corresponding to the RH range from 0.67 to 32 % [22]. The Cu(111) surface is thus much more *hydrophobic* than the Cu(110) surface.

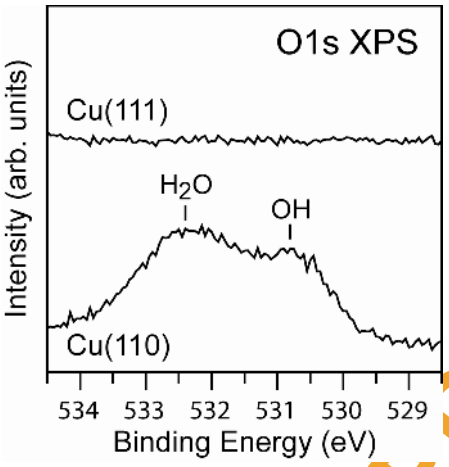

Figure 5. O 1s XPS spectra measured in the presence of 1 Torr water vapor on two different Cu surfaces at 295 K (a relative humidity of 5.0 %): Cu(110) and Cu(111). The partial coverages of OH and H_2O on Cu(110) in 1 Torr H_2O at 295 K are 0.34 and 0.68 ML, respectively. The gas phase water peak is observed around 536 eV (not shown). The incident photon energy was 735 eV.

The different wettability on two Cu surfaces, (110) and (111), stems from a difference in the activation barrier for the OH formation (i.e., water dissociation). The lower dissociation barrier on Cu(110) than Cu(111) is demonstrated by the present experiments at near ambient conditions from the fact that OH species are present on Cu(110), but not on Cu(111) (see figure 5). It is also supported by previous UHV studies showing that thermally-induced water dissociation occurs on Cu(110) [45, 49, 50, 52], but not on Cu(111) [43, 44]. The absence of OH groups on Cu(111) in the present experiments ($p(H_2O)$= 1 Torr, T= 268 – 333 K) indicates kinetic limitations of water dissociation on Cu(111) under these conditions. The dissociation barrier in the low coverage limit has been determined experimentally from kinetic measurements of the water-gas shift reaction on Cu(110) and Cu(111) to be ~0.87 eV [63] and ~1.17 eV [64], respectively. These values are in good agreement with the calculated dissociation barriers of water monomers on Cu surfaces using density functional theory (DFT) calculations [65].

The difference in dissociation barriers of water on the two Cu surfaces is explained by the linear Brønsted-Evans-Polanyi (BEP) relationship [66, 67] between activation energies and enthalpy changes for dissociative adsorption [68-70]: a larger thermodynamical driving force (ΔH) leads to a lower activation barrier for similar reactions. The water dissociation reaction is exothermic ($\Delta H < 0$) on Cu(110) [62], but thermoneutral ($\Delta H = 0$) on Cu(111) [71, 72]. Hence the different wetting properties of Cu(110) and Cu(111) surfaces manifest the essential role of surface OH groups in water adsorption on metals surfaces.

3.1.5 Water adsorption on the oxygen precovered Cu(111)

It is well known that preadsorbed oxygen on metal surfaces can induce water dissociation [16, 17]. Figure 6 shows O 1s XPS spectra for a partially oxygen-covered Cu(111) surface measured in UHV and in the presence of 1 Torr water vapor at 295 K. The preadsorbed atomic O (θ= 0.12) on Cu(111) reacts with 1 Torr water vapor ($H_2O + O \rightarrow$

2OH) to form a mixed OH and H_2O layer. The hydrophilicity of the Cu(111) surface is thus generated by the formation of OH groups that stabilize water molecules through strong hydrogen bonds, similar to what we observe on the Cu(110) surface.

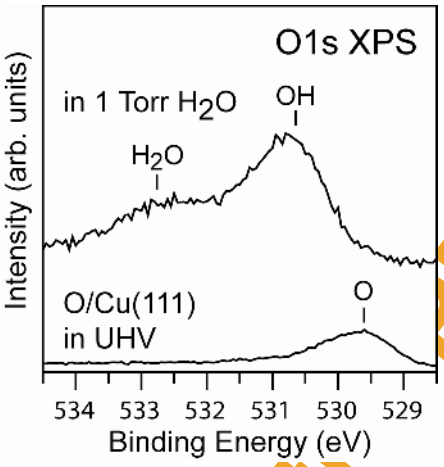

Figure 6. O 1s XPS spectra for a partially oxygen-covered Cu(111) surface (θ_O= 0.12) measured in ultrahigh vacuum (UHV) and in the presence of 1 Torr water vapor at 295 K (5.0 % RH). The partial coverages of OH and H_2O on Cu(111) in 1 Torr H_2O at 295 K are 0.26 and 0.17 ML, respectively. The gas phase water peak is observed around 536 eV (not shown). The incident photon energy was 735 eV.

3.2 Water on oxides

3.2.1 Introduction

Titanium dioxide, especially rutile (110) surface, is one of the most extensively studied oxide surfaces [17, 73, 74]. The particular interest in water chemistry on TiO_2 surfaces has been stimulated by their important properties such as the photochemical production of hydrogen from water and the photo-induced hydrophilicity [75, 76].

The interaction of water with TiO_2(110) has been extensively studied in UHV. It has been shown that water chemistry on TiO_2(110) is largely influenced by the presence of oxygen vacancies in the rows of bridging oxygen atoms [17, 73, 74]. The dissociation of water molecules at bridging oxygen vacancy sites has been directly imaged by scanning tunneling microscopy (STM) and atomic force microscopy (AFM) in UHV [77-82]. On the defect-free perfect TiO_2(110) surface, in contrast, many experimental studies in UHV suggest that water does not dissociate [17, 74, 77, 78]; different theoretical calculations predict both dissociative (at least at low coverages) [83-86] and molecular adsorption [87-89] on the defect-free surface. The current disagreement between experiments and theoretical calculations may be due to the existence of high activation barriers that hinder dissociation and molecular rearrangement [86], raising the question of whether thermodynamic equilibrium is reached in low temperature UHV studies. In addition, oxygen vacancy defects playing an important role in water dissociation on TiO_2(110) may be healed and absent under ambient conditions. Therefore, despite its great importance, information on the adsorbed water layer on the TiO_2(110) surface under realistic ambient conditions is scarce. Simple questions such as the amount of adsorbed water in equilibrium with vapor and the structure of the first water layer in contact

with the surface, including the possibility of dissociation into OH and H groups remain largely unanswered. Therefore the nature of adsorption sites for water on TiO_2(110) and whether water dissociation is required for water adsorption is still elusive under ambient conditions. To answer these questions, we have studied the adsorption of water on the TiO_2(110) surface under near ambient conditions of pressure and temperature ($p(H_2O) \leq$ 1.5 Torr, T= 265 – 800 K), using ambient pressure XPS.

3.2.2 Water chemistry on TiO_2(110) at near ambient conditions

First we characterize the clean TiO_2(110) surface in vacuum using XPS. We have found that a small amount of O-vacancy defects are always present on the clean TiO_2(110) surface after surface preparation, even after cooling in O_2. These O-vacancy defects are revealed with characteristic features in the Ti 2p and O 1s regions as well as in the valence band [74, 90]. Figure 7 shows (a) Ti $2p_{3/2}$ and (b) O 1s XPS spectra for the defective TiO_2(110) surface that was prepared by Ar^+ sputtering, annealing to 900 – 950 K in vacuum. In the Ti 2p region, a shoulder feature is observed at the lower binding-energy side of the Ti^{4+} $2p_{3/2}$ peak due to the reduced Ti species (Ti^{3+} and/or Ti^{2+}) [90, 91]. In the O 1s region, a small component is observed at about 1 eV higher binding energy than the lattice oxygen peak at 530.5 eV. This is assigned to O atoms next to vacancy sites because this feature is not observed on the stoichiometric surfaces. In addition, a defect state appears in the band gap at about 1 eV below the conduction band (not shown), which is attributed to the occupied 3d states of Ti^{3+} [92, 93]. The defect concentration is determined by the Ti^{3+}/Ti^{4+} ratio under consideration of the electron mean free path and analyzer geometry, as described in Ref. [90]. The TiO_2(110) surfaces presented in figure 7a and b have defect concentrations of 0.156 ML and 0.125 ML, respectively.

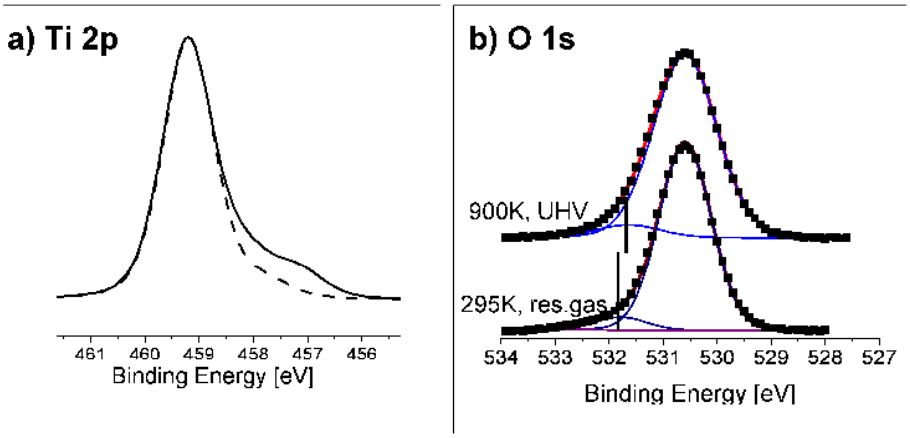

Figure 7. (a) Ti $2p_{3/2}$ XPS spectra of defective TiO_2(110) before water exposure (solid line) and after introduction of 10^{-4} Torr H_2O at 420 K (dashed line). The defective TiO_2(110) surface is prepared by Ar^+ sputtering, followed by annealing to 950 K in vacuum. The incident photon energy was 630 eV. (b) O 1s XPS spectra of defective TiO_2(110) measured at 900 K in vacuum (top curve) and measured after cooling down to 295 K in a residual gas atmosphere (mainly water) of 10^{-8} Torr (bottom curve). The incident photon energy was 690 eV.

After the defective TiO_2(110) is exposed to 10^{-4} Torr water (see figure 7a), the $Ti^{3+,2+}$ shoulder in the Ti $2p_{3/2}$ peak

is readily quenched except for a very small residual amount (< 0.03 ML), which we attribute to bulk defects [74]. Concurrent with the change in Ti 2p, in the O 1s region a new peak appears at ~1.3 eV higher binding energy than the lattice oxygen peak. This new feature is assigned to OH groups at bridging sites [94, 95]. In figure 7b, the coverage of OH saturates at around 0.25 ML. The OH coverage of 0.25 ML is indeed expected from the initial defect concentration of 0.125 ML, if each water molecule dissociates into an OH group that fills the vacancy (V_{bridge}), and a H atom that forms an identical species by binding to another bridging O site (O_{bridge}): $H_2O + V_{bridge} + O_{bridge} = 2OH_{bridge}$. For defect concentrations lower than 0.125 ML, the final OH coverage is also lower, but always twice the defect concentration. The following experiments were performed on a surface with an initial defect concentration of 0.125 ML.

Next we investigate the hydroxylation and water adsorption on the TiO_2(110) surface under near ambient conditions of pressure and temperate. Figure 8 shows O 1s XPS difference spectra on TiO_2(110) recorded at four different sample temperatures in a constant pressure of 0.4 Torr H_2O vapor (isobar). The XPS spectra in the isobar were obtained with decreasing sample temperature. To show the changes in O 1s XPS spectra clearly, the difference spectrum is obtained by subtracting the XPS spectrum measured in UHV before water exposure from each XPS spectrum at different sample temperatures after normalization with the lattice oxygen peak.

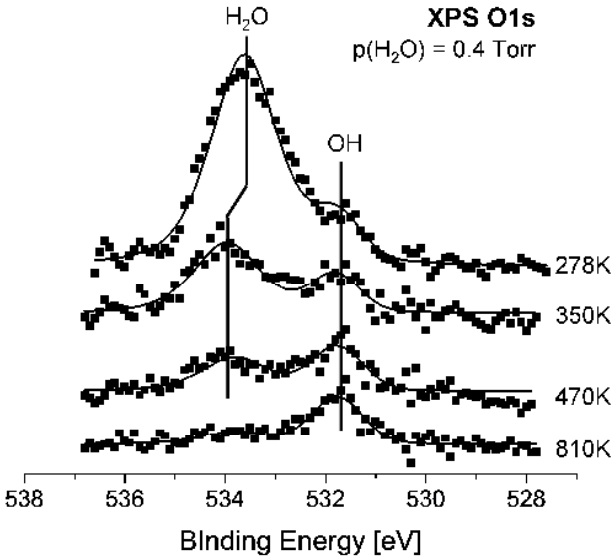

Figure 8. O 1s XPS difference spectra on TiO_2(110) recorded in the presence of 0.4 Torr water vapor at sample temperatures of 810, 470, 350, 278 K. The difference spectra are obtained by subtracting the XPS spectrum measured in UHV before water exposure from each XPS spectrum at different sample temperatures in 0.4 Torr H_2O after normalization with the lattice oxygen peak. The gas-phase water peak observed around 536 eV in the raw O 1s XPS spectra is cancelled out by subtraction of the fitting line for the well-separated gas phase peak. The dots are the experimental data after the subtraction procedures explained above and the thin solid line is the result from a least-square peak-fitting procedure. The incident photon energy was 690 eV.

As seen in figure 8, the OH feature already saturates at 810 K in 0.4 Torr H_2O. As the sample temperature

decreases, a second peak appears at ~3.5 eV higher binding energy with respect to the lattice oxygen peak. This peak can be attributed to either hydroxyl [94] or molecular water [96] at Ti^{4+} sites between bridging O rows. As shown in figure 7b and further evidenced by the experimental results below, the saturation coverage of OH is twice the initial coverage of oxygen vacancies. This indicates that water dissociation on TiO_2(110) occurs only at O-vacancy defects and does not proceed at the fivefold coordinated Ti^{4+} sites. We thus attribute this feature to molecular water adsorbed on the fivefold coordinated Ti^{4+} sites. With a further decrease in temperature, the coverage of adsorbed water increases with its O 1s XPS peak shifting to lower binding energies by ~0.5 eV.

Figure 9a shows the coverages of OH and H_2O obtained from the same isobar experiment that provided the data in figure 8. The OH coverage is constant at 0.25 ML over the temperature range from 800 K to 275 K, which is twice the initial defect concentration of 0.125 ML. Water adsorbs on the hydroxylated surface until its coverage equals that of the OH groups. Above a water coverage of 0.25 ML, water coverage increases more rapidly. Between 0.25 ML and 2 ML water coverage, the O 1s XPS peak of adsorbed water shifts towards lower binding energies by ~0.5 eV, with most of the shift taking place below 1 ML (see figure 8).

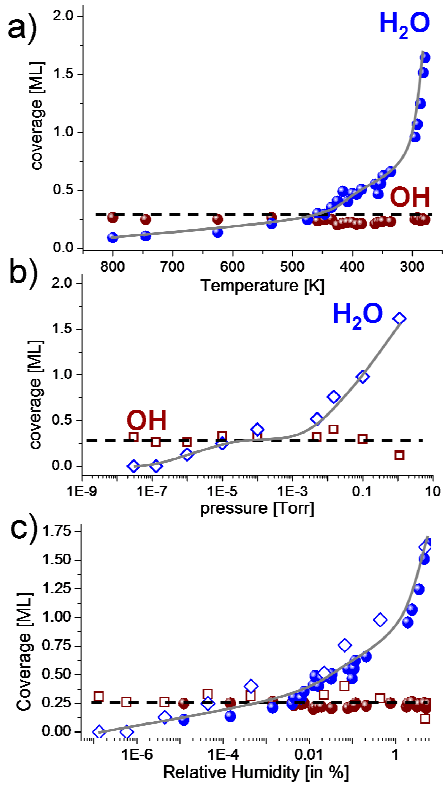

Figure 9. Uptake curves of OH and H_2O on TiO_2(110) obtained from (a) isobar (p= 0.4 Torr) with decreasing sample temperature and (b) isotherm (T= 298 K) with increasing water pressure. (c) The same data are plotted as a function of relative humidity. Filled symbols are for isobar and open symbols are for isotherm. Both results collapse into the same curve, demonstrating that the surface and gas phase are in thermodynamic equilibrium. Dashed and solid lines are inserted as a visual aid.

Qualitatively similar results are obtained from isotherms, as shown by the room temperature data set in figure 9b.

Both isobar and isotherm uptake curves collapse into one when the data are plotted as a function of relative humidity (RH), as shown in figure 9c. This confirms a thermodynamic equilibrium between vapor and surface in the present experiments. A point that is worth considering is that in the isobar experiments the sample temperature is changing while that of the vapor remains constant at room temperature. The temperature used to compute the relative humidity is that of the sample. The error in having two different temperatures is however very small, due to the fact that the surface temperature is in the exponential of the desorption rate, while that of the gas is in the form $T^{-0.5}$ in the expression for the impingement rate with the surface.

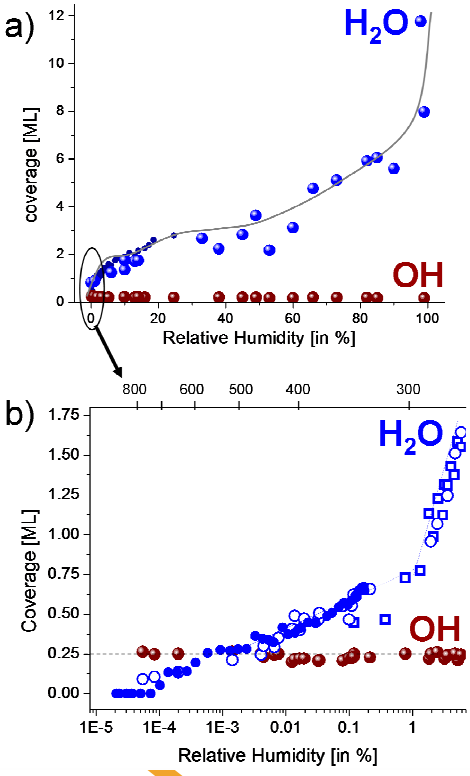

Figure 10. (a) Coverage of OH and H_2O on TiO_2(110) obtained from different isobars (10^{-2} to 1.5 Torr) as a function of relative humidity. Small dots are data obtained with the heater sample holder and large dots with the Peltier sample holder. (b) Enlarged view of the low relative humidity region (data from three different isobars: filled dots, 0.01 Torr; open dots, 0.4 Torr; open squares, 1 Torr). The temperature scale at the top corresponds to the 0.4 Torr isobar. Notice the change of the x-axis from linear to logarithmic in the two plots. There is a plateau at 0.25 ML in (b), when the coverage of water equals that of OH.

Figure 10a shows the uptake curves of OH and H_2O over a wide range of relative humidity. Details of the OH and H_2O coverages at low relative humidity are shown in the enlarged plot of figure 10b, which summarizes the results of three different experimental isobars. Similar to what we observed in figure 9, at the very low relative humidities from 5×10^{-5} % to 3.5×10^{-3} %, the coverage of adsorbed water increases to be equal to the initial OH coverage (0.25 ML), where the uptake curve shows an inflexion followed by a small plateau. Another kink is observed around 0.75 ML. The coverage of water increases rapidly between 0 and 25 % RH, with inflections at approximately 12 and

25 % RH, which correspond to 2 ML and 3 ML, respectively. Between 25 and ~60 % RH water coverage changed slowly, and then increased rapidly when approaching 100 % RH. Note that the coverage of OH species remains constant at twice the initial defect concentration (0.25 ML) at all RHs.

To summarize, water adsorption on the TiO_2(110) surface occurs in distinct steps. First, water molecules dissociate at O-vacancies in bridge sites, producing a stoichiometric amount of OH bridge groups equal to twice the initial vacancy concentration: $H_2O + V_{bridge} + O_{bridge} = 2OH_{bridge}$ This step takes place even at very low relative humidities. These OH_{bridge} groups act as nucleation sites that anchor water molecules to form strongly bound OH-H_2O complexes. The OH-H_2O complexes continue to act as nucleation centers for further water adsorption. The wetting properties of TiO_2(110) are thus driven by moderate amounts (<0.25 ML) of strongly attractive OH sites that nucleate water molecules.

4. Discussion

The present results on the adsorption of water on Cu(110), Cu(111), and TiO_2(110) at near ambient conditions demonstrate that the presence of surface OH groups plays an essential role in wetting properties of surfaces. Here we compare the hydroxylation and water adsorption on these surfaces, and discuss the stability of H_2O-OH complex and its generality on other surfaces.

We observe a general behavior in the adsorption of water on the surfaces studied here at near ambient conditions; hydroxylation precedes water adsorption. We find a difference in the coverage of OH and the onset of water adsorption on these surfaces. The onset of water adsorption is defined as the point where adsorbed molecular water roughly equal to 0.1 monolayer can be detected by XPS. The coverage of OH on TiO_2(110) saturates at twice the initial defect concentration, since the hydroxylation on TiO_2(110) occurs only at O-vacancy defects. On the Cu(110) surface, OH groups are formed on the terrace and its coverage saturates around 0.33 ML. On the Cu(111) surface, hydroxylation is kinetically hindered under the present conditions except for the oxygen preadsorbed surface. The onsets of water adsorption on Cu(110) and TiO_2(110) are ~2.5×10^{-2} % and ~1×10^{-5} % RH, respectively. Water adsorption is not observed on the clean Cu(111) surface up to 32 % RH.

We believe that the stability of H_2O-OH complexes is a general phenomenon on metal and oxide surfaces. Indeed, previous UHV studies have shown that the mixed H_2O:OH layers on metal surfaces exhibit distinct water desorption states in the 200-240 K range, well above those from molecularly intact layers in the 160 – 180 K range [16, 17]. Examples include a full range of metal substrates such as Cu(110) [48, 52], Ag(110) [97], Ni(110) [98], Pt(111) [99], Ru(0001) [100, 101], Rh(111) [102], and Pd(111) [103]. On Cu(110), for instance, the peak desorption temperatures of water in the mixed H_2O:OH layer are 200 and 235 K in UHV [48, 52], which are higher than the desorption temperature of 175 K in the molecularly intact water layer [45, 48, 52]. The H_2O desorption at 235 K from the 1:1 H_2O:OH phase on Cu(110) leads to the desorption barrier (i.e., the adsorption energy) of 0.18 ± 0.01 eV (for $\upsilon = 10^{15\pm1}$ s^{-1}) higher than that from the molecularly intact layer on Cu(110) (T_{des} = 175 K) [48]. The H_2O desorption process requires breaking bonds to the Cu substrate as well as to neighboring adsorbates (H_2O or OH). The larger desorption barrier (adsorption energy) in the mixed H_2O:OH layer originates from the H_2O-OH

H-bonds that is ~0.18 eV stronger than the H_2O- H_2O H-bonds. This is quantitatively in good agreement with a recent theoretical work on the Pt(111) surface where the H_2O-OH H-bond strength is ~0.2 eV stronger than the H_2O-H_2O H-bond [104, 105].

In the case of TiO_2(110), previous TPD studies have reported the desorption feature of water at about 270 K , which is ascribed to water molecules in the first monolayer [96, 106-108]. These water molecules in the first layer on TiO_2(110) may be stabilized by the H-bonds with OH groups at defects sites, which could be present in various amounts depending on the surface preparation. The adsorption energy (desorption barrier) for the first monolayer water on TiO_2(110) (270 K) is larger than that for water in the 1:1 H_2O:OH phase on Cu(110) (235K). This is consistent with the earlier onset of water adsorption on TiO_2(110) than Cu(110).

Here we discuss the interaction between OH and H_2O on metal and oxide surfaces in terms of their Brønsted acid and base character. The nature of the H-bonds between OH and H_2O is predominantly electrostatic [109]. For instance, OH^- ions in solution have a formal negative charge, which makes it a strong H-bond acceptor but a weak H-bond donor towards H_2O (i.e., Brønsted base). This strong H_2O(donor)-OH(acceptor) nature results in the O-O bond length asymmetry of long OH donating H-bonds and short OH accepting H-bonds [110]. In addition, OH species adsorbed on metal surfaces generally carry a partial negative charge, which depends delicately on the interaction with the substrate [105, 111-113]. Therefore, as analogous to OH^- in solution, OH species adsorbed on metal surfaces is of Brønsted base character. The strong H_2O-OH H-bond at metal surfaces is thus the H_2O(donor)-OH(acceptor) bond, while the reverse situation yields a very weak bond. This is consistent with theoretical results on donor-acceptor properties of OH species towards H_2O on Pt(111) [104, 105, 113] and Rh(111) [114]. In contrast, the bridging OH groups on the TiO_2(110) surface have been argued to be of Brønsted acid character [115]. Recent AFM study on the TiO_2(110) surface has shown that the bridging OH groups formed at defect sites are positively charged using a charged AFM tip [79]. Therefore, the strong H_2O-OH H-bond on the TiO_2(110) surface should be the OH(donor)- H_2O(acceptor) bond, which is the reverse of the H_2O-OH H-bond on metal surfaces.

These considerations show that the formation of OH groups plays an important role in water adsorption (wetting) on surfaces. The stabilization of H_2O with the surface OH groups originates from the H_2O-OH H-bonding interaction that is stronger than the H_2O- H_2O H-bonding interaction. The different wettability of solid surfaces originates from the difference in the kinetic barrier for OH formation and the number and nature of OH groups on the surface.

5. Summary and future outlook

Ambient pressure XPS was applied to the study of water adsorption on the surface of metals and metal oxides including Cu(110), Cu(111), TiO_2(110) under pressures and temperatures near those of the ambient conditions. The synchrotron-based ambient pressure XPS setup, combining differential pumping and electrostatic focusing, enables in situ XPS measurements at pressures above 5 Torr. We have obtained quantitative insight into the molecularly intact and dissociative adsorption of water on metal and oxide surfaces under adsorption-desorption equilibrium

conditions at near ambient water partial pressures.

We have found that surface OH groups play an essential role in water adsorption (wetting) on solid surfaces. On all the surfaces studied here, water adsorption takes place on the hydroxylated surface. Surface OH groups act as anchoring sites for adsorbed water molecules through H_2O-OH H-bonding that is stronger than the H_2O- H_2O H-bonding. The difference in the kinetic barrier for OH formation and the number and nature of OH groups on surfaces results in the different wettability of surfaces. For instance, the Cu(111) surface is much more *hydrophobic* than the Cu(110) surface at near ambient conditions. This can be explained by a higher activation barrier for water dissociation on Cu(111) than on Cu(110). We have shown that the Cu(111) surface becomes *hydrophilic* by the formation of OH groups induced by preadsorbed oxygen. On the TiO_2(110) surface, the OH formation occurs only at O-vacancy defects and thus its coverage is limited to twice the initial vacancy concentration. The acid or base character of the OH species in the OH-H_2O complex is different on Cu and on TiO_2(110); OH groups on Cu(110) and Cu(111) are of Brønsted base character, but OH groups on TiO_2(110) are of Brønsted acid character. The difference in the number and nature of OH groups on surfaces would be responsible for the difference in the onset of water adsorption on surfaces. From the detailed comparison of water chemistry on Cu(110) between at near ambient conditions and in UHV at low temperatures, we have found a very good agreement in the local chemical environments (XPS binding energies), H_2O:OH ratios, and stability order of surface phases on Cu(110). Futhermore, analysis of the adsorption-desorption equilibrium of the surface phase observed at near ambient conditions shows that the kinetic information obtained in UHV at low temperature is well extrapolated to conditions of ambient pressures and temperatures.

Here we briefly mention those areas which, in our opinion, will present exciting scientific opportunities for future in-situ XPS work.

First of all, it is highly desirable to extend the present in-situ XPS study of water adsorption on surfaces to not only other metals and oxides but also ionic solids, semiconductors, biological materials. The chemical-specific quantification of surface compositions by in-situ XPS allows us to correlate water adsorption with the presence of surface OH groups. This will deepen our understanding how the kinetic barrier for OH formation and the number and nature of OH groups on surfaces affect water adsorption, and will provide further evidence of the general importance of surface OH groups in water adsorption on solid surfaces.

One of the most important areas for in-situ XPS studies is to investigate surface chemical reactions involving water under the reaction conditions. In heterogeneous catalysis, it is often found that the presence of water on surfaces significantly alter the selectivity and activity of catalytic reactions [1, 2, 14, 15]. Since the H-bonding interactions between water (and/or OH) and other molecules adsorbed on surfaces largely affect surface chemical kinetics, it is important to have a general understanding of how H-bonding influences various activation barriers for elementary steps of surface chemical reactions.

An important and complementary technique to XPS is X-ray absorption spectroscopy (XAS), which can be performed easily using the same experimental setup. We have recently demonstrated that O K-edge XAS spectra contains information on the structure of water in the bulk liquid phase [116], and when adsorbed as a monolayer on metal surfaces in UHV [47, 117]. These studies show that O K-edge XAS is very sensitive to H-bonding

environments of water molecules. However, the structure of thin film water in equilibrium with ambient pressure water vapor is still largely unknown and only recently some initial results are being obtained [118]. The fundamental questions that can be addressed by in-situ XAS include the structure of the thin water film and its evolution as a function of film thickness, role of the substrate, and the important question of how many layers are required for water to reach its bulk structure.

It is noteworthy that the structure of water molecules on surfaces could be different between UHV and low temperature conditions and the more real life conditions of pressure (a few Torr) and temperature (near 0 ^{o}C). In a water monolayer on metal surfaces, for example, water molecules are connected by H-bonds to form a hexagonal honeycomb structure where half of the water molecules are adsorbed in an oxygen-down configuration and the other half take a configuration of pointing a free (i.e., non H-bonded) OH either to a vacuum ("H-up") or to a metal surface ("H-down"). The recent UHV studies at low temperatures (<140 K) have provided the detailed insights into the branching of water between "H-up" and "H-down" configurations on several metal surfaces; water is adsorbed predominantly in the "H-down" configuration on Pt(111) [117, 119] and on Ru(0001) [100, 120-122], while the mixed "H-up" and "H-down" configurations are found for water monolayer on Cu(110) (H-down: H-up = ~2:1) [47] and on Rh(111) (H-down: H-up = ~1.3:1) [123]. The DFT calculations show a small energy difference in the order of 0~40 meV between "H-up" and "H-down" configurations [72, 124]. Indeed, the energy difference is experimentally estimated to be as small as 3~5 meV in the mixed configuration phases on Cu(110) and Rh(111) [47, 123]. In addition, the kinetic barrier to flip the water configuration between "H-up" and "H-down" has been reported to be as low as 76 meV on Pt(111) [124] and 55 meV on Ru(0001) [125]. Therefore, the population ratio between "H-up" and "H-down" species at realistic conditions (ambient pressures and elevated temperatures) is expected to be very different from that at ideal conditions (UHV and low temperatures).

Acknowledgements

This work was supported by the National Science Foundation under Contract No. CHE-0431425 (Stanford Environmental Molecular Science Institute); by the Office of Biological and Environmental Research, Materials and Chemical Sciences Divisions of the Lawrence Berkeley Laboratory, of the U.S. Department of Energy under Contract No. DE-AC02-05CH11231 through the Advanced Light Source and the Stanford Synchrotron Radiation Laboratory, and under the auspices of the President's Hydrogen Fuel Initiative; the Swedish Foundation for Strategic Research and the Swedish Natural Science Research Council. GK thanks the Alexander-von-Humboldt foundation for financial support.

References

[1] King D A and Woodruff D P (eds) 1982 *The Chemical Physics of Solid Surfaces and Heterogeneous Catalysis* vol 4 Fundamental Studies of Heterogeneous Catalysis (Amsterdam: Elsevier)

[2] Chorkendorff I and Niemantsverdriet J W 2003 *Concepts of Modern Catalysis and Kinetics* (Weinheim: Wiley-VCH)

[3] Bligaard T and Nørskov J K 2008 *Chapter 4 Heterogeneous Catalysis* (Amsterdam: Elsevier) in *Chemical Bonding at Surfaces and Interfaces*: Nilsson A, Pettersson L G M and Nørskov J K (eds)

[4] Brown Jr G E, Henrich V E, Casey W H, Clark D L, Eggleston C, Felmy A, Goodman D W, Grätzel M, Maciel G, McCarthy M I, Nealson K H, Sverjensky D A, Toney M F and Zachara J M 1999 *Chem. Rev.* **99** 77

[5] Brown Jr G E, Trainor T P and Chaka A M 2008 *Chapter 7 Geochemistry of Mineral Surfaces and Factors Affecting Their Chemical Reactivity* (Amsterdam: Elsevier) in *Chemical Bonding at Surfaces and Interfaces*: Nilsson A, Pettersson L G M and Nørskov J K (eds)

[6] Zondlo M A, Hudson P K, Prenni A J and Tolbert M A 2000 *Annu. Rev. Phys. Chem.* **51** 473

[7] Girardet C and Toubin C 2001 *Surf. Sci. Rep.* **44** 159

[8] Weaver M J and Gao X 1993 *Annu. Rev. Phys. Chem.* **44** 459

[9] Marković N M and Ross Jr P N 2002 *Surf. Sci. Rep.* **45** 117

[10] Strasser P and Ogasawara H 2008 *Chapter 6 Surface Electrochemistry* (Amsterdam: Elsevier) in *Chemical Bonding at Surfaces and Interfaces*: Nilsson A, Pettersson L G M and Nørskov J K (eds)

[11] Leygraf C and Graedel T 2000 *Atmospheric Corrosion* (New York: Wiley)

[12] Wiggins P M 1990 *Microbiol. Rev.* **54** 432

[13] Kasemo B 2002 *Surf. Sci.* **500** 656

[14] Bergeld J, Kasemo B and Chakarov D V 2001 *Surf. Sci.* **495** L815

[15] Date M and Haruta M 2001 *J. Catal.* **201** 221

[16] Thiel P A and Madey T E 1987 *Surf. Sci. Rep.* **7** 211

[17] Henderson M A 2002 *Surf. Sci. Rep.* **46** 1

[18] Verdaguer A, Sacha G M, Bluhm H and Salmeron M 2006 *Chem. Rev.* **106** 1478

[19] Briggs D and Seah M P (eds) 1990 *Practical Surface Analysis* 2nd ed (England: New York) vol. 1-Auger and X-Ray Photoelectron Spectroscopy

[20] Mårtensson N and Nilsson A 1995 *Chapter 3 High-Resolution Core-Level Photoelectron Spectroscopy of Surfaces and Adsorbates* Springer Series in Surface Science 35 (Berlin: Springer-Verlag) in *Application of Synchrotron Radiation; High-Resolution Studies of Molecules and Molecular Adsorbates on Surfaces* : Eberhardt W (eds)

[21] Nilsson A 2002 *J. Electron. Spectrosc. Relat. Phenom.* **126** 3

[22] Yamamoto S, Andersson K, Bluhm H, Ketteler G, Starr D E, Schiros T, Ogasawara H, Pettersson L G M, Salmeron M and Nilsson A 2007 *J. Phys. Chem. C* **111** 7848

[23] Andersson K, Ketteler G, Bluhm H, Yamamoto S, Ogasawara H, Pettersson L G M, Salmeron M and Nilsson A 2007 *J. Phys. Chem. C* **111** 14493

[24] Andersson K, Ketteler G, Bluhm H, Yamamoto S, Ogasawara H, Pettersson L G M, Salmeron M and Nilsson A *submitted to J. Am. Chem. Soc.*

[25] Ketteler G, Yamamoto S, Bluhm H, Andersson K, Starr D E, Ogletree D F, Ogasawara H, Nilsson A and Salmeron M 2007 *J. Phys. Chem. C* **111** 8278

[26] Siegbahn H and Siegbahn K 1973 *J. Electron. Spectrosc. Relat. Phenom.* **2** 319

[27] Fellner-Feldegg H, Siegbahn H, Asplund L, Kefve P and Siegbahn K 1975 *J. Electron. Spectrosc. Relat. Phenom.* **7** 421

[28] Siegbahn H 1985 *J. Phys. Chem.* **89** 897

[29] Joyner R W, Roberts M W and Yates K 1979 *Surf. Sci.* **87** 501

[30] Watanabe I, Flanagan J B and Delahay P 1980 *J. Chem. Phys.* **73** 2057

[31] Ballard R, Jones J, Read D and Inchley A 1986 *Chem. Phys. Lett.* **127** 149

[32] Ruppender H J, Grunze M, Kong C W and Wilmers M 1990 *Surf. Interface. Anal.* **15** 245

[33] Kelly M A, Shek M L, Pianetta P, Gür T M and Beasley M R 2001 *J. Vac. Sci. Technol. A* **19** 2127

[34] Pantförder J, Pöllmann S, Zhu J F, Borgmann D, Denecke R and Steinrück H P 2005 *Rev. Sci. Instrum.* **76** 014102

[35] Ogletree D F, Bluhm H, Lebedev G, Fadley C S, Hussain Z and Salmeron M 2002 *Rev. Sci. Instrum.* **73** 3872

[36] Bluhm H, Andersson K, Araki T, Benzerara K, Brown G E, Dynes J J, Ghosal S, Gilles M K, Hansen H C, Hemminger J C, Hitchcock A P, Ketteler G, Kilcoyne A L D, Kneedler E, Lawrence J R, Leppard G G, Majzlam J, Mun B S, Myneni S C B, Nilsson A, Ogasawara H, Ogletree D F, Pecher K, Salmeron M, Shuh D K, Tonner B, Tyliszczak T, Warwick T and Yoon T H 2006 *J. Electron. Spectrosc. Relat. Phenom.* **150** 86

[37] Bluhm H, Hävecker M, Ihmann K, Kleimenov E, Teschner D, Ogletree D F, Salmeron M, Knop-Gericke A and Schlögl R 2007 *to be submitted to Rev. Sci. Instrum.*

[38] Warwick T, Andresen N, Comins J, Kaznacheyev K, Kortright J B, McKean J P, Padmore H A, Shuh D K, Stevens T and Tyliszczak T 2004 *AIP Conference Proceedings* **705** 458

[39] Petersen H 1982 *Optics Comm.* **40** 402

[40] Follath R and Senf F 1997 *Nucl. Instr. Methods Phys. Res. A* **390** 388

[41] Coulman D J, Wintterlin J, Behm R J and Ertl G 1990 *Phys. Rev. Lett.* **64** 1761

[42] Jensen F, Besenbacher F, Lægsgaard E and Stensgaard I 1990 *Phys. Rev. B* **41** 10233

[43] Hinch B J and Dubois L H 1992 *J. Chem. Phys.* **96** 3262

[44] Bovensiepen U, Gahl C and Wolf M 2003 *J. Phys. Chem. B* **107** 8706

[45] Andersson K, Gómez A, Glover C, Nordlund D, Öström H, Schiros T, Takahashi O, Ogasawara H, Pettersson L G M and Nilsson A 2005 *Surf. Sci.* **585** L183

[46] Yamada T, Tamamori S, Okuyama H and Aruga T 2006 *Phys. Rev. Lett.* **96** 036105

[47] Schiros T, Haq S, Ogasawara H, Takahashi O, Öström H, Andersson K, Pettersson L G M, Hodgson A and Nilsson A 2006 *Chem. Phys. Lett.* **429** 415

[48] Bange K, Grider D E, Madey T E and Sass J K 1984 *Surf. Sci.* **136** 38

[49] Spitzer A and Lüth H 1982 *Surf. Sci.* **120** 376

[50] Spitzer A and Lüth H 1985 *Surf. Sci.* **160** 353

[51] Kubota J, Kondo J, Domen K and Hirose C 1993 *Surf. Sci.* **295** 169

[52] Polak M 1994 *Surf. Sci.* **321** 249

[53] Kolovos-Vellianitis D and Küppers J 2003 *J. Phys. Chem. B* **107** 2559

[54] Ammon C, Bayer A, Steinrück H P and Held G 2003 *Chem. Phys. Lett.* **377** 163

[55] Clendening W D, Rodriguez J A, Campbell J M and Campbell C T 1989 *Surf. Sci.* **216** 429

[56] Brown D E, George S M, Huang C, Wong E K L, Rider K B, Smith R S and Kay B D 1996 *J. Phys. Chem.* **100** 4988

[57] Brinkley D, Dietrich M, Engel T, Farrall P, Gantner G, Schafer A and Szuchmacher A 1998 *Surf. Sci.* **395** 292

[58] Daschbach J L, Peden B M, Smith R S and Kay B D 2004 *J. Chem. Phys.* **120** 1516

[59] Delval C and Rossi M J 2004 *Phys. Chem. Chem. Phys.* **6** 4665

[60] King D A 1975 *Surf. Sci.* **47** 384

[61] Attard G and Barnes C 1998 *Surfaces* (Oxford: Oxford University Press)

[62] Ren J and Meng S 2006 *J. Am. Chem. Soc.* **128** 9282

[63] Nakamura J, Campbell J M and Campbell C T 1990 *J. Chem. Soc. Faraday Trans.* **86** 2725

[64] Campbell C T and Daube K A 1987 *J. Catal.* **104** 109

[65] Jiang L, Wang G C, Cai Z S, Pan Y M and Zhao X Z 2004 *J. Mol. Struct. (Theochem)* **710** 97

[66] Brønsted J N 1928 *Chem. Rev.* **5** 231

[67] Evans M G and Polanyi M 1938 *Trans. Faraday Soc.* **34** 11

[68] Hammer B and Nørskov J K 2000 *Adv. Catal.* **45** 71

[69] Pallassana V and Neurock M 2000 *J. Catal.* **191** 301

[70] Michaelides A, Liu Z P, Zhang C J, Alavi A, King D A and Hu P 2003 *J. Am. Chem. Soc.* **125** 3704

[71] Kandoi S, Gokhale A A, Grabow L C, Dumesic J A and Mavrikakis M 2004 *Catal. Lett.* **93** 93

[72] Michaelides A, Alavi A and King D A 2004 *Phys. Rev. B* **69** 113404

[73] Henrich V E and Cox P A 1994 *The Surface Science of Metal Oxides* (Cambridge: Cambridge University Press)

[74] Diebold U 2003 *Surf. Sci. Rep.* **48** 53

[75] Honda K and Fujushima A 1972 *Nature* **238** 37

[76] Wang R, Hashimoto K, Fujishima A, Chikuni M, Kojima E, Kitamura A, Shimogoshi M and Watanabe T 1997 *Nature* **388** 431

[77] Wendt S, Schaub R, Matthiesen J, Vestergaard E K, Wahlstrom E, Rasmussen M D, Thostrup P, Molina L M, Lægsgaard E, Stensgaard I, Hammer B and Besenbacher F 2005 *Surf. Sci.* **598** 226

[78] Wendt S, Matthiesen J, Schaub R, Vestergaard E K, Lægsgaard E, Besenbacher F and Hammer B 2006 *Phys. Rev. Lett.* **96** 066107

[79] Lauritsen J V, Foster A S, Olesen G H, Christensen M C, K¨uhnle A, Helveg S, Rostrup-Nielsen J R, Clausen B S, Reichling M and Besenbacher F 2006 *Nanotechnology* **17** 3436

[80] Bikonda O, Pang C L, Ithnin R, Muryn C A, Onishi H and Thornton G 2005 *Nature Mat.* **5** 189

[81] Pang C L, Sasahara A, Onishi H, Chen Q and Thornton G 2006 *Phys. Rev. B* **74** 073411

[82] Zhang Z, Bondarchuk O, Kay B D, White J M and Dohnálek Z 2006 *J. Phys. Chem. B* **110** 21840

[83] Fahmi A and Minot C 1994 *Surf. Sci.* **304** 343

[84] Goniakowski J and Gillan M J 1996 *Surf. Sci.* **350** 145

[85] Lindan P J D, Harrison N M and Gillan M J 1998 *Phys. Rev. Lett.* **80** 762

[86] Lindan P J D and Zhang C 2005 *Phys. Rev. B* **72** 075439

[87] Stefanovich E V and Trong T T 1999 *Chem. Phys. Lett.* **299** 623

[88] Schaub R, Thostrup P, Lopez N, Lægsgaard E, Stensgaard I, Nørskov J K and Besenbacher F 2001 *Phys. Rev. Lett.* **87** 266104

[89] Harris L A and Quong A A 2004 *Phys. Rev. Lett.* **93** 086105

[90] Wang L Q, Baer D R and Engelhard M H 1994 *Surf. Sci.* **320** 295

[91] Mayer J T, Diebold U, Madey T E and Garfunkel E 1995 *J. Electron. Spectrosc. Relat. Phenom.* **73** 1

[92] Henrich V E, Dresselhaus G and Zeiger H J 1976 *Phys. Rev. Lett.* **36** 1335

[93] Zhang Z, Jeng S P and Henrich V E 1991 *Phys. Rev. B* **43** 12004

[94] Sham T K and Lazarus M S 1979 *Chem. Phys. Lett.* **68** 426

[95] Wang L Q, Baer D R, Engelhard M H and Shultz A N 1995 *Surf. Sci.* **344** 237

[96] Hugenschmidt M B, Gamble L and Campbell C T 1994 *Surf. Sci.* **302** 329

[97] Bange K, Madey T E, Sass J K and Stuve E M 1987 *Surf. Sci.* **183** 334

[98] Benndorf C and Madey T E 1988 *Surf. Sci.* **194** 63

[99] Clay C, Haq S and Hodgson A 2004 *Phys. Rev. Lett.* **92** 046102

[100] Clay C, Haq S and Hodgson A 2004 *Chem. Phys. Lett.* **388** 89

[101] Faradzhev N S, Kostov K L, Feulner P, Madey T E and Menzel D 2005 *Chem. Phys. Lett.* **415** 165

[102] Wagner F T and Moylan T E 1987 *Surf. Sci.* **191** 121

[103] Clay C, Cummings L and Hodgson A 2007 *Surf. Sci.* **601** 562

[104] Karlberg G S and Wahnström G 2004 *Phys. Rev. Lett.* **92** 136103

[105] Karlberg G S and Wahnström G 2005 *J. Chem. Phys.* **122** 194705

[106] Henderson M A 1996 *Surf. Sci.* **355** 151

[107] Henderson M A 1996 *Langmuir* **12** 5093

[108] Henderson M A 1998 *Surf. Sci.* **400** 203

[109] Jeffrey G A 1997 *An Introduction to Hydrogen Bonding* (Oxford: Oxford University Press)

[110] Botti A, Bruni F, Imberti S, Ricci M A and Soper A K 2004 *J. Chem. Phys.* **120** 10154

[111] Koper M T M and van Santen R A 1999 *J. Electroanal. Chem.* **472** 126

[112] Seitsonen A P, Zhu Y, Bedürftig K and Over H 2001 *J. Am. Chem. Soc.* **123** 7347

[113] Schiros T, Näslund L Å , Andersson K, Gyllenpalm J, Karlberg G S, Odelius M, Ogasawara H, Pettersson L G M and Nilsson A 2007 *J. Phys. Chem. C* **111** 15003

[114] Vassilev P, Koper M T M and van Santen R A 2002 *Chem. Phys. Lett.* **359** 337

[115] Boehm H P 1971 *Disc. Faraday Soc.* **52** 264

[116] Wernet P, Nordlund D, Bergmann U, Cavalleri M, Odelius M, Ogasawara H, Näslund L Å, Hirsch T K, Ojamäe L, Glatzel P, Pettersson L G M and Nilsson A 2004 *Science* **304** 995

[117] Ogasawara H, Brena B, Nordlund D, Nyberg M, Pelmenschikov A, Pettersson L GM and Nilsson A 2002 *Phys. Rev. Lett.* **89** 276102

[118] Verdaguer A, Weis C, Oncins G, Ketteler G, Bluhm H and Salmeron M 2007 *Langmuir* **23** 9699

[119] Haq S, Harnett J and Hodgson A 2002 *Surf. Sci.* **505** 171

[120] Andersson K, Nikitin A, Pettersson L G M, Nilsson A and Ogasawara H 2004 *Phys. Rev. Lett.* **93** 196101

[121] Denzler D N, Hess C, Dudek R, Wagner S, Frischkorn C, Wolf M and Ertl G 2003 *Chem. Phys. Lett.* **376** 618

[122] Haq S, Clay C, Darling G R, Zimbitas G and Hodgson A 2006 *Phys. Rev. B* **73** 115414

[123] Beniya A, Yamamoto S, Mukai K, Yamashita Y and Yoshinobu J 2006 *J. Chem. Phys.* **125** 054717

[124] Meng S, Wang E G and Gao S 2004 *Phys. Rev. B* **69** 195404

[125] Meng S, Wang E and G, Frischkorn C, Wolf M and Gao S 2005 *Chem. Phys. Lett.* **402** 384